INTERNATIONAL JOURNAL FOR NUMERICAL METHODS IN BIOMEDICAL ENGINEERING
Int. J. Numer. Meth. Biomed. Engng. 2012; **28**:1028–1042
Published online 25 June 2012 in Wiley Online Library (wileyonlinelibrary.com). DOI: 10.1002/cnm.2499

Inspiration from nature: dynamic modelling of the musculoskeletal structure of the seahorse tail

Tomas Praet [1,*,†], Dominique Adriaens [2], Sofie Van Cauter [1], Bert Masschaele [3], Matthieu De Beule [1] and Benedict Verhegghe [1]

[1] *IBiTech-bioMMeda, Department of Civil Engineering, Ghent University, Ghent, Belgium*
[2] *Evolutionary Morphology of Vertebrates, Department of Biology, Ghent University, Ghent, Belgium*
[3] *Centre for X-ray Tomography (UGCT), Ghent University, Ghent, Belgium*

SUMMARY

Technological advances are often inspired by nature, considering that engineering is frequently faced by the same challenges as organisms in nature. One such interesting challenge is creating a structure that is at the same time stiff in a certain direction, yet flexible in another. The seahorse tail combines both radial stiffness and bending flexibility in a particularly elegant way: even though the tail is covered in a protective armour, it still shows sufficient flexibility to fully function as a prehensile organ. We therefore study the complex mechanics and dynamics of the musculoskeletal system of the seahorse tail from an engineering point of view. The seahorse tail derives its combination of flexibility and resilience from a chain of articulating skeletal segments. A versatile dynamic model of those segments was constructed, on the basis of automatic recognition of joint positions and muscle attachments. Both muscle structures that are thought to be responsible for ventral and ventral–lateral tail bending, namely the median ventral muscles and the hypaxial myomere muscles, were included in the model. Simulations on the model consist mainly of dynamic multi-body simulations. The results show that the sequential structure of uniformly shaped bony segments can remain flexible because of gliding joints that connect the corners of the segments. Radial stiffness on the other hand is obtained through the support that the central vertebra provides to the tail plating. Such insights could help in designing biomedical instruments that specifically require both high bending flexibility and radial stiffness (e.g. flexible stents and steerable catheters). Copyright © 2012 John Wiley & Sons, Ltd.

Received 15 December 2011; Revised 22 May 2012; Accepted 23 May 2012

KEY WORDS: seahorse; dynamic modelling; multi-body dynamics; inspiration from nature

1. INTRODUCTION

Billions of years of selective pressures have forced organisms to come up with robust and efficient evolutionary solutions to a whole range of real-world problems. Through evolution, subtle changes in functionality are tested on their impact on the organismal fitness and, thereafter, either reinforced or rejected. Such an optimization procedure is in many ways comparable with design cycles that are used in engineering. No wonder then that throughout history, many scientists and engineers turned to nature for inspiration on technological advances, while considering nature to be an enormous database of field-tested solutions. Nowadays, this ‘design from nature’ approach finds a renewed interest, even for advanced engineering applications [1–4].

*Correspondence to: Tomas Praet, IBiTech-bioMMeda, Department of Civil Engineering, Ghent University, Ghent, Belgium.

†E-mail: tomas.praet@ugent.be

Research into nature's designs often sprouts from the mind of engineers or scientists that are struck with amazement by a specific adaptation in nature. In our case, it were the specialised adaptations of seahorses (genus *Hippocampus*) that caught our eye. Unlike other bony fish, these members of the family Syngnathidae swim and feed in an upright position [5–7], while using dorsal and, to a lesser extent, pectoral fin undulation for propulsion [8–10] (Figure 1). Unable to rely on a usually much stronger caudal fin for propulsion, the seahorse is considered to be a relatively slow swimming fish, which is unlikely to outrun any predatory fish. Seahorses can, however, avoid predation using crypsis, as they developed camouflage according to their specific environments. Besides camouflage, the seahorse also relies on skeletal plating, which covers the body [11], instead of scales, which can be found in most fish species. This strong and tough body plating extends over the entire tail and likely makes seahorses more resilient to predatory bites. Nevertheless, the seahorse tail is still sufficiently flexible to function as a prehensile (grasping and holding) organ [11]. By bending the tail ventrally into a spiral, the seahorse manages to hold on to a mate or to objects on the sea floor (mostly corals or seagrass), so that this slow swimming animal can remain hidden without being carried away by strong currents [7, 9, 12–14].

To allow such high bending flexibility, the plating of the seahorse tail shows a specialised articulation [9, 11], driven by a complex system of muscles, tendons and bones, which determines the characteristics of the tail motion. The seahorse tail can actively bend in ventral direction (prehension), combined ventral–lateral direction (helical bending) and dorsal direction (overstretching) [11, 13, 15, 16].

In general, structures that are very flexible in particular directions, but still stiff, strong and tough in other directions, are frequently required in engineering. For example, the steel cables of an elevator need to be strong and stiff to cope with the weight of the elevator and counter weight, without dangling up and down like a bungee cord, while maintaining sufficient flexibility to be wound up around the pulley. The observed combination of high radial stiffness and bending flexibility, which is typical for the seahorse tail, is also highly valued in engineering. For example, stent grafts in the lower extremities will require a combination of high radial stiffness (to keep the artery open for sufficient blood flow) and bending flexibility (to cope with knee bending and soft tissue deformations).

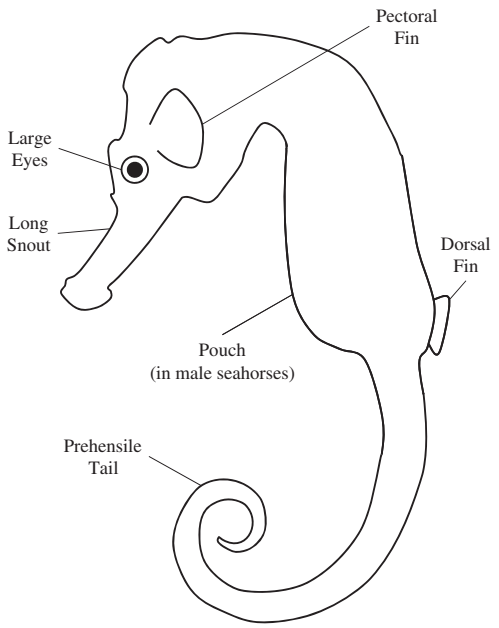

Figure 1. Some seahorse characteristics. The dorsal and pectoral fins are used for propulsion, whereas the prehensile tail holds on to objects on the seabed. The large eyes, long snout and forward bending of the head give the seahorse a distinct horse-like appearance, hence its name.

DOI: 10.1002/cnm

Combining such often conflicting mechanical properties can be challenging. Looking at nature's solutions on these issues can provide a much needed fresh perspective, while knowing that the provided solutions have been rigorously field-tested. Most biomechanically relevant features of the seahorse tail have previously been described in literature [9, 11, 16], yet to the best of our knowledge, no kinematic or dynamic model of the seahorse tail has previously been published by other authors.

In this paper, we present results of our ongoing construction of a versatile dynamic model of the seahorse tail. In a previous study, we simulated the kinematics of a limited amount of caudal segments at small ventral bending [17]. The new model can simulate the dynamics of entire tail bending, up to very high bending in both ventral and ventral–lateral directions. Studying the fundamentals of the biomechanics of the seahorse tail is the first step towards understanding the processes that are involved in efficiently combining strength and flexibility in complex structures. Obtaining fundamental biomechanical insights can indeed be considered as the basics for any biomimetic engineering process. The insights that we gather from our analyses should lead to inspiration for both the development and optimization of instruments in biomedical engineering, such as an innovative design for steerable catheters for stent delivery.

2. BASIC SEAHORSE TAIL ANATOMY

2.1. Geometry of the bony elements

Several micro-CT scans were acquired from a specimen of an adult seahorse, species *Hippocampus reidi* (also known as longsnout seahorse or slender seahorse), with voxel sizes ranging from 7.05 to 50 μm, depending on the region of interest. A tube voltage of 70 kV was used together with a detector with a 127-μm pixel pitch. Scans were taken with the tail fixed in three different positions: curled, stretched and overstretched, in order to compare the position of the bony elements in different tail positions. To study the muscle structure and connective tissues in more detail, two other adult specimens of the *Hippocampus reidi* species were additionally scanned using a high-resolution phase contrast synchrotron X-ray scanner at European Synchrotron Radiation Facility in Grenoble. A resolution of 2048 × 2048 pixels and voxel size of 7.46 μm was obtained using a FreLoN CCD camera. The images were segmented using 3D Slicer 3.6.

The skeleton of the seahorse tail consists of a chain of uniformly shaped segments, which caudally decrease in size, as indicated in Figure 2. Towards the tail tip, the segments gradually become more 'inclined', as the dorsal side of the segment becomes more distally stretched and the ventral

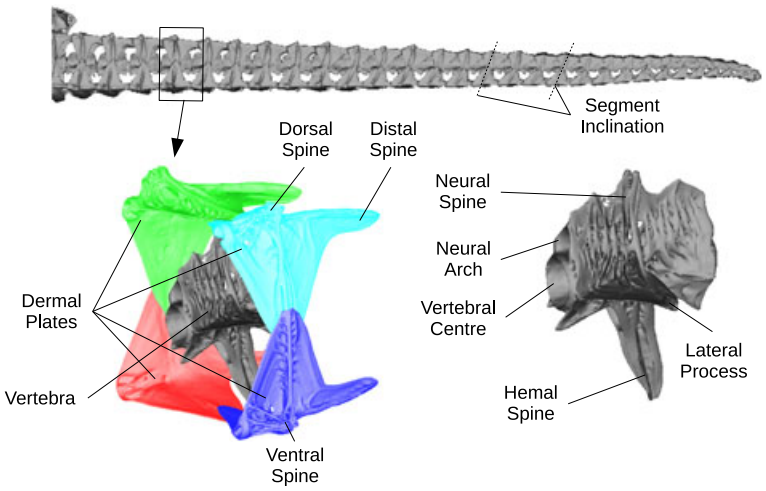

Figure 2. Geometry of the skeletal segments in the seahorse tail. Each of the uniformly shaped segments consists of one vertebra surrounded by four dermal plates.

DOI: 10.1002/cnm

side becomes more proximally stretched. Each of the skeletal segments consists of five articulating bony elements (2):

(i) A central vertebra
(ii) A left dorsal dermal plate
(iii) A right dorsal dermal plate
(iv) A left ventral dermal plate
(v) A right ventral dermal plate

The uniform shape throughout the tail is evident for both the caudal vertebrae [9] and the dermal plates. The central amphicoelous vertebra has four processes that stretch out towards the dermal plates: a hemal spine, a neural spine and two lateral processes [11] (Figure 2). The dermal plates have processes that distally extend into a groove on the next dermal plate in the chain of tail segments (distal spines, Figure 2). The dorsal dermal plates have a dorsal spine, whereas the ventral dermal plates have a ventral spine. These dorsal and ventral spines are the only spines in the seahorse tail that are not involved in the formation of a joint.

2.2. The joints of the seahorse tail

Each segment of the seahorse tail contains 13 joints, eight of which act like gliding joints, the other five act like ball-and-socket joints (Figure 3).

The distal ends of the lateral processes of the central vertebra are connected to the dorsal dermal plates by a joint in which all three rotational degrees of freedom are free (Figure 3(A)). This means that the joint basically behaves like a ball-and-socket joint, although the socket of the joints between the lateral processes of the vertebra and the dorsal dermal plates is not always clearly visible on the medial surface of the dermal plates and sometimes even completely absent. Presumably, the socket is predominantly formed by connective tissues, like a syndesmosis joint. The hemal spine connects to the ventral dermal plates, although the distal end of the hemal spine is located at some distance of the ventral plates. The joint, however, is established through thick subdermal collagen layers that connect the tip of the hemal spine to the dermal plates [11], which results in a rather flexible joint.

The joints between the amphicoelous vertebrae allow for quite some rotation around all three axis (Figure 3(B)). In between the vertebrae and the connective tissues interconnecting the vertebrae are the remnants of the larval spinal column (i.e. the notochord). Some limited gliding of the joint is therefore possible.

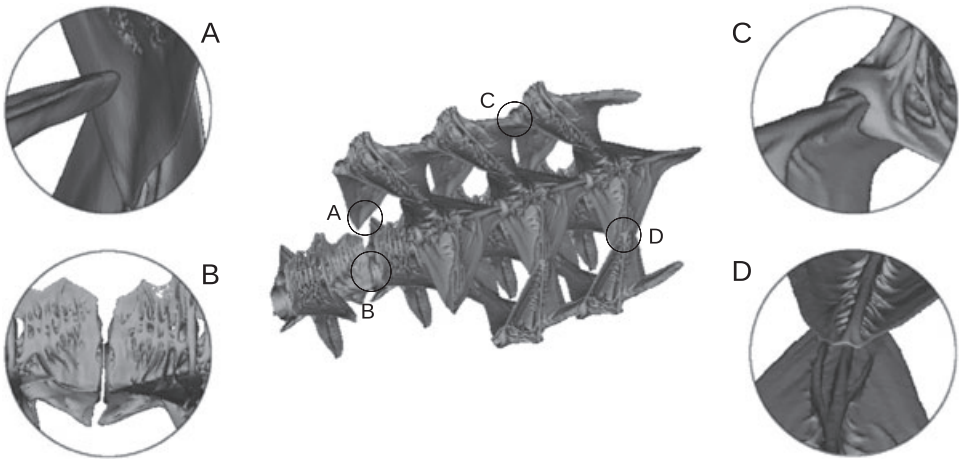

Figure 3. The joints in the seahorse tail can loosely be considered to be ball-and-socket joints (A and B) or gliding joints (C and D): ball-and-socket joints between vertebrae and dermal plates (A) and between subsequent vertebrae (B); gliding joints between subsequent dermal plates (C) and between dermal plates within the same segment (D).

DOI: 10.1002/cnm

Subsequent dermal plates are connected by gliding joints. The distal spine of the anterior dermal plate fits into a proximal groove in the posterior dermal plate (Figure 3(C)). The distal spine is shaped like a rail, which limits the movement of both bony elements in relation to each other substantially: only linear motion in the longitudinal direction shows low resistance. The tight fit of the joint even limits the rotation around the anteroposterior axis. The surface of the distal spine is slightly curved in the longitudinal direction, which will make the bony elements rotate slightly when the joint is compressed or elongated. The groove in the dermal plates ends rather abruptly, so at a certain penetration of the distal spine, resistance against further penetration of the plates rises quickly. This is the position where the gliding joint is compressed to its maximum.

The dermal plates have bony 'ridges' on the otherwise flat outer surfaces near the joints between dermal plates of the same segment (Figure 3(D)). These ridges provide a small rail over which the other plate can slide. The rounded shape with relatively low curvature, however, creates a gliding joint that is much less tight than the gliding joints between subsequent dermal plates. Both rotation and sliding along a varying direction is still possible up to a certain degree. We believe that the ridges on the dermal plates actually play a more important role in increasing the bending stiffness of the dermal plates, rather than providing a strong supporting rail for the joint. At the lateral gliding joints, the plates have a preferential stacking (ventral on top of dorsal dermal plate), whereas the stacking at other gliding joints within a segment seems to vary without a clear pattern.

2.3. The muscle structure of the seahorse tail

The structure and mechanics of fishes' muscular system is still poorly understood [18]. In general, the trunk muscles in fish are arranged in longitudinal series of short muscles, called myomere muscles, separated by collagenous sheets, called myosepta [19] (Figure 4). This structure of alternating myomeres and myosepta is folded into complex shapes that differ between species [18, 20]. The myosepta are usually folded into several longitudinally directed cones [18–20], resulting in a typical W-shaped pattern in sagittal slices of the trunk muscles and a concentric structure in transverse slices, a condition also found in most syngnathids [21]. A recent study indicated a complex organisation of connective tissue sheets that is unique for seahorses [21]. Most fish have a horizontal septum (a horizontal layer of collagen fibres) that divides the muscles into hypaxial muscles (lower halve of the body) and epaxial muscles (upper halve of the body). This is also the case in seahorses, as indicated in Figure 4.

Given the upright position and the unique locomotion of seahorses, it should come as no surprise that the myomere muscle structure differs significantly from that of most other fishes, including other syngnathids [21]. This is especially clear for the seahorses' hypaxial myomere muscles (HMM), which span an increased number of vertebrae compared with other fish genera. The myosepta that separate the HMM fibres are arranged in a more or less parallel configuration (Figure 4), rather than the more common concentric configuration. The myosepta can therefore span up to eight segments, proximally starting from the medial–ventral position, over the lateral–ventral position (where the thick ventral tendons attach to the medial surface of the ventral dermal

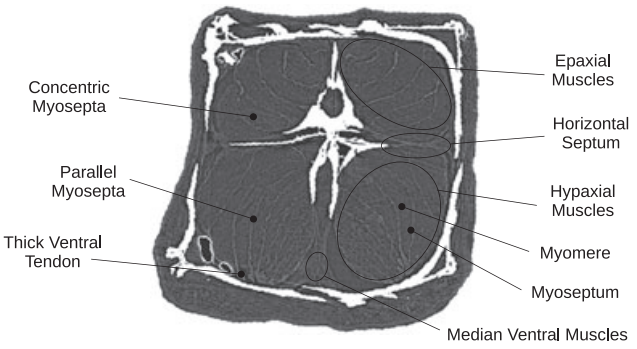

Figure 4. Muscle structure in the seahorse tail on a transverse synchrotron scan slice.

DOI: 10.1002/cnm

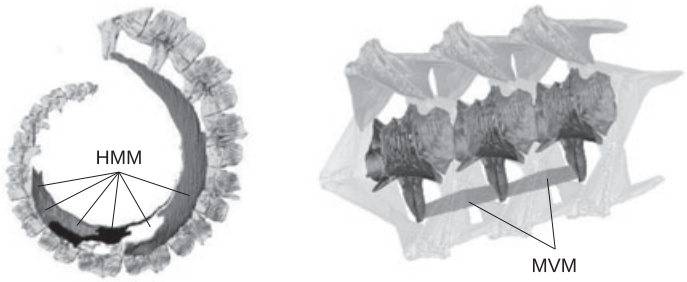

Figure 5. Three-dimension reconstruction of the median ventral muscles (MVMs) and the myosepta of the hypaxial myomere muscles (HMMs).

plate) and distally ending at the lateral position (Figure 5). The longest myomeres can be found near the middle of the tail, whereas the shortest myomere muscles can be found near the base and the tip of the tail [11, 16]. The epaxial muscles on the other hand still show to some extent the concentric configuration that we see in most fish species [21].

The HMM appear to be used predominantly for fast and forceful tail bending [11], as in grasping. The lateral position of the HMM allows them to cause both combined ventral–lateral bending (upon unilateral contraction) and pure ventral bending (upon bilateral contraction). The median ventral muscles (MVMs) on the other hand are located on the most ventral side within the midsagittal plane (Figure 4), connecting the hemal spines of adjacent vertebrae (Figure 5). This conveniently provides a rather large moment arm for tail bending. The midsagittal position of the MVM indicates that they can only be used for ventral bending. The MVM are likely used for slower, more sustained tail bending [11], as in holding on to an object. The HMM and MVM are assumed to be the only muscles that actively contribute to ventral tail bending in seahorses. From observations, we learned that the seahorse can control the ventral tail bending meticulously, almost to the point where a single segment can be bent independently of the others. It would seem like the seahorse makes use of the MVM rather than the HMM in those specific cases.

3. DYNAMIC MODEL GENERATION

The methodology to construct the dynamic models was deliberately kept flexible and versatile, so that parametric studies could be conducted in the future, and other scans of possibly other seahorse species could easily be incorporated. With the description in the previous section, the position of the joints and the muscle attachments were determined automatically from the skeletal surface models using dedicated Python scripts in pyFormex, which is an in-house developed open-source software package for generating, transforming and manipulating large geometrical models of 3D structures by sequences of mathematical operations (www.pyformex.org).

3.1. Skeletal elements

Using 3D Slicer 3.6, detailed 3D surface models were constructed of a single segment of the stretched tail that was deemed to be representable for the other uniformly shaped segments. Special care was given to the smoothing of the surface models. As the dermal plates are connected by gliding joints, local roughness of the mesh can influence simulation results dramatically. However, standard Laplacian smoothing will result in significant shrinkage of the surface models. We therefore used a slightly adapted version of the Humphrey's Classes algorithm [22], which is available in pyFormex, to obtain nicely smoothed surface models of the bony elements in the seahorse tail, without significant loss of shape or volume. The surface models were obtained from scans with the tail in stretched position, as this was assumed to be the resting position of the seahorse tail.

An approximative representation of the other tail segments was thereafter derived from the surface models by appropriate geometric transformations (scaling and skewing), as to avoid the time-consuming process of manually segmenting the large amount of skeletal elements in the tail (145 in

DOI: 10.1002/cnm

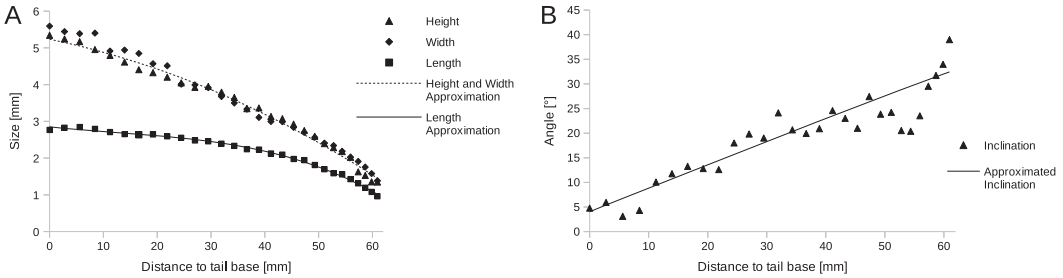

Figure 6. Scaling (A) and inclination (B) approximation throughout the seahorse tail. The tail length is the length measured on a stretched tail starting from the most proximal segment. Approximations are fitted on third-degree polynomial for the segment length, second-degree polynomial for the height and width, and linear regression for the inclination. The Pearson product–moment correlation coefficients are 0.996 for the length, 0.988 for the width, 0.991 for the height of the segment and 0.845 for the segment inclination.

total). Automated segmentation was not possible because of the small distance between the dermal plates near the gliding joints: this distance is much smaller than the obtainable resolutions so that even automatic segmentation algorithms fail to separate the bony elements. The inclination or skewness of a tail segment is taken as the angle that the central 'ridge' of the dorsal dermal plate makes with the transverse plane. The skewness appears to be small for the proximal segments but becomes important for the caudal segments, possibly because the tail curvature is highest near the tail tip during ventral bending.

The scaling and inclination (skewing) parameters were calculated on the basis of polynomial approximations that best fitted measurements on the CT scans (Figure 6). The size of the segments along the dorsoventral axis (height) and the left-right axis (width) are measured in the transverse plane and are almost equal to each other throughout the tail. They are therefore estimated by the same quadratic approximation. In the longitudinal direction (length), the segment size is determined as the distance between the subsequent vertebral centres. The length of the segments decreases towards the tail tip although slower than the height and width. As a result, the most caudal segments have an almost cubic shape, whereas the more proximal segments are longitudinally compressed. For the segment length, a third-degree polynomial approximation was used. The skewness on the other hand is approximated by linear regression, with caudal segments showing a greater spreading in measured skewness, because the central ridge of the lateral joints becomes rather flat on the smaller segments. With the use of the approximated scaling and skewing values, a generic surface model of the seahorse tail is constructed.

3.2. Joints and muscles

To allow for easy comparison between models generated from different scans, the segmented tail segment is automatically rotated into a standardised position. Using the principal axes of inertia of the vertebral surface model, the direction of the lateral processes is determined and the model is rotated to align this lateral axis to the Z-axis. Thereafter, the longitudinal axis (determined as the second principal axis) is taken as the X-axis and the dorsoventral axis as the Y-axis.

The position of the joints between the vertebra and the dermal plates can then be found by averaging the extreme points of the processes on the vertebra with the nearest point on the appropriate dermal plate. To determine the position of the joint between subsequent vertebrae, we calculate the geometric centre of the inner circle that is found by intersecting the vertebra with a transverse plane, that is located at 10% of the total longitudinal length of the vertebra, for both the proximal vertebra (cutting with a distal transverse plane) and the distal vertebra (cutting with a proximal transverse plane). The joint is then taken at the average of those two points.

The attachment points of the MVMs is found by cutting off the hemal spine at its base, rotating it to a standardised position based on the principle axes (of the separated spine) and calculating points on the midsagittal plane at 90% of the total length of the hemal spine (Figure 7(A)). This value was

DOI: 10.1002/cnm

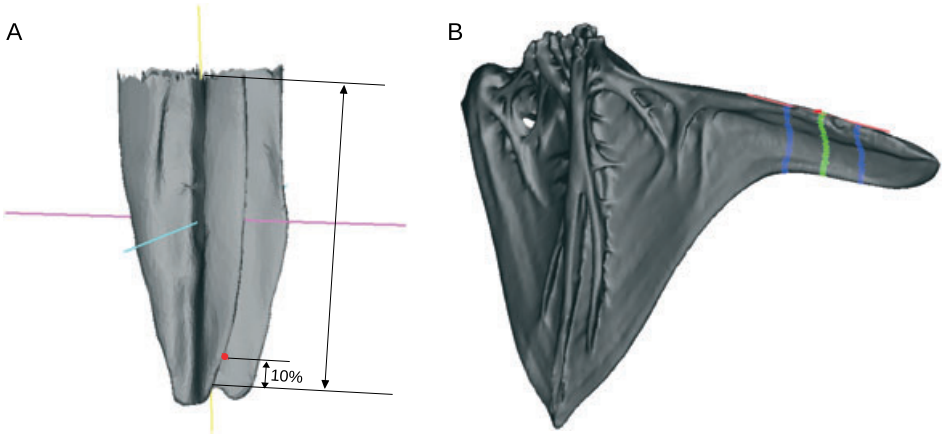

Figure 7. (A) Example of muscle attachment calculation. The attachment points of the MVM to the hemal spine (red dot) is set at 10% of the total length of the spine. Those lengths are measured along the principal axes of inertia of the hemal spine (in yellow, cyan and magenta in this figure).(B) Example of how the gliding joint positions and their main direction are determined. The position of the gliding joint between adjacent left dorsal dermal plates (red point) is determined as the most left and dorsal point of the plate, on a transverse plane positioned at the initial penetration of the distal spine. Main gliding direction of the joint (red line) is calculated on the basis of points around the anticipated penetration for the provided muscle contractions.

assumed to be a good approximation on the basis of measurement of several MVM attachments on the sagittal synchrotron slices.

For the dermal plates, the gliding joint positions within the same segment are found by averaging the extreme points on both plates that make up the joint. Because this point is always formed by the central ridge of the plates, the position of the average point is a good approximation of the real position of the joint. The direction of the lateral gliding joint follows the skewness of the segments (because the skewness was calculated on the basis of the direction of the central ridge of the lateral joints). Gliding joints between subsequent dermal plates follow the curvature of the surface of the distal spines (Figure 7(B)). This curvature is approximated for the anticipated joint displacement, as the current modelling technique does not yet allow us to implement non-linear joint paths. We saw no benefit in including the total length of the distal spines, as even at maximal ventral tail bending (to a point where the MVMs are maximally contracted), the distal processes of the dorsal dermal plates are still within their respective distal grooves, except for some of the most distal segments.

3.3. Generating simplified dynamic models

Input files for the dynamic analyses are written using scripts in pyFormex, on the basis of parameters provided by the user. As an entire tail model can hold up to a 145 skeletal elements and 380 joints, the dynamic models were initially kept rather simple to reduce the solving time. For most analyses, each detailed surface model of the skeletal elements was substituted by a simplified rigid body that consists of the centre of mass of the detailed model, attachment points of the joints and attachment points of the muscles involved in ventral tail bending. Necessary parameters for dynamic analyses, such as mass and moments of inertia, are inherited by the simplified geometries. For determining inertia, a general density of 1.8 g/cm^3 was assumed, which is a typical value for fish bone [23]. The density is used only to calculate the masses, as buoyancy and gravity are assumed to cancel each other out. In those cases that deformable models were used, an isotropic linear elastic material model was used with a Young's module of 6.48 GPa and a Poisson ratio of 0.3. These are general material properties for acellular bone of fish ribs, which were adopted from literature [24]. The small size (maximally 8 mm per segment) and irregular shape of the seahorse tail bones make it difficult to conduct reliable material tests.

DOI: 10.1002/cnm

An example of the generated model is demonstrated in Figure 8. Starting from the general geometries, simplified geometries are generated, incorporating only the points that are necessary for basic dynamic analyses. The joints are currently modelled as non-linear elastic connectors (springs). The elasticity that is given to the joints can be adapted and is dependent upon local axis directions. To improve the stability of the model, a small linear elasticity value of 1 μN/mm is given in directions where the joint elasticity could be assumed to be close to zero, such as the elongation of the joints between subsequent dermal plates. The elasticity of the compression of the joints between subsequent dermal plates is estimated by separate finite element simulations. The two skeletal elements of the joints are considered to be deformable bodies with linear isotropic material properties and frictionless contact. With the use of displacement-driven analyses, the joint is compressed and the required force is monitored. Assuming that all joint elasticity is stored in bone deformation, a non-linear elasticity response of the joint is obtained, as shown in Figure 9. These joint stiffnesses are used as the first approximation, until we can quantify the effect of soft tissues and passive muscles.

Stiffness of the other joints is estimated relative to the stiffness of the joints between subsequent dermal plates. More realistic values will be incorporated once reliable tests on the tail of a seahorse specimen have been conducted. The gliding joints between the skeletal elements of one segment are given an elasticity of 1 μN/mm in their main direction and 0.01 N/mm for the other two directions.

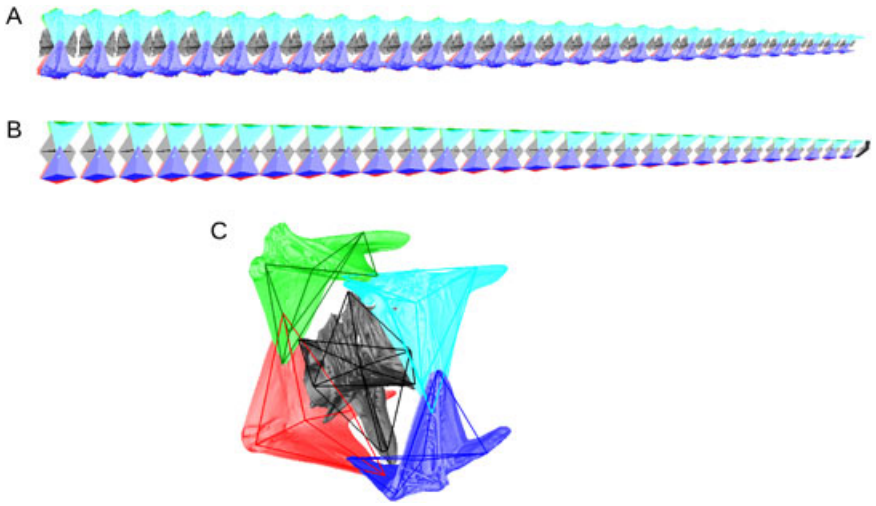

Figure 8. Model of the seahorse tail with realistic (A) and simplified (B) geometries. The simplified geometries are calculated on the basis of the automatic recognition of geometrical features (C).

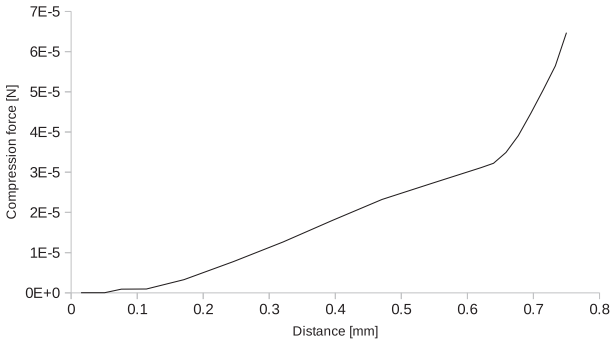

Figure 9. Non-linear response when compressing the joint between subsequent dorsal dermal plates. Around 0.65-mm joint compression, a rather sudden rise in stiffness can clearly be distinguished. This is the point where the distal spine reaches maximal intrusion into the groove of the distal plate. Further compression necessitates significant deformation of the distal spine.

DOI: 10.1002/cnm

Rotational elasticity is taken as 0.01 N/degree. Finally, for the ball-and-socket joints, rotational elasticity is taken very low (1 μN/degree) and translational elasticity is taken high (100 N/mm), except for the more flexible joints between subsequent vertebrae (10 N/mm).

The resting position of the joints is determined as the joint positions in a fully stretched tail. Whether this tail position is the real resting position of the seahorse tail is debatable. Personal observations on anaesthetised seahorses indicate that the resting position of the seahorse tail can be variable (from straight to slightly curved) although this position can be altered significantly with minimal effort.

The muscles are, at this stage, modelled as simple beams that can elongate and contract. Future models will include the epaxial myomere muscles as passive muscles at ventral tail bending. Currently, upon muscle contraction (time dependent shortening of the beams), energy is stored in the joints as potential energy. This potential energy is distributed between the joints so that, at each time step, an equilibrium arises. Some kinetic energy originates as well during the movement, but the kinetic energy is monitored to stay less than 1% at all times so that the final result of the simulations is actually almost time independent. Because tail movement in seahorses is typically slow (in the order of seconds) and the masses are low (as the tail has small dimensions), the assumption to minimise the kinetic energy is reasonable. Drag forces that act on the tail are probably of more importance to the tail dynamics but are ignored in the current model. Because our final goal is to develop biomedical applications rather than developing an extremely accurate seahorse tail model, this approach was deemed to be sufficiently accurate at this stage.

The small size of seahorses makes it difficult to measure reaction forces and internal forces. Using electromyography to measure muscle activation is even more difficult: the muscles involved in tail bending are very small and numerous. So, instead of imposing muscle forces on the model, changes in length of the muscles are applied on the model. General estimation of these contractions are based on visual observations on seahorses grasping on to a horizontal dowel.

The presented model is confronted with an inherent problem: the high number of rigid bodies (around 150 for a full tail model) makes the use of some usual multi-body simulation software impractical. We therefore opted to use the multi-body functionalities embedded in ABAQUS 6.11 (Dassault Systèmes, Vélizy-Villacoublay, France), a finite element solver that is frequently used in engineering. This may not seem to be the most preferable approach for dynamic simulations in biomechanics, but it does present us with some very interesting opportunities: we can include deformable bodies in the model, as well as contacting surfaces (to get a more accurate modelling of the joints). Preliminary models use frictionless contact, although future models will take friction into account. We can conduct both dynamic (taking inertias into account) and standard (not taking inertias into account) analyses. This approach proved to be nicely scalable, which comes in handy for the large number of segments. The way that the multi-body dynamics are treated results in a O(n) process, meaning that a doubling of parts in the model will roughly result in a doubling of the computing time.

Combining the parametric model generation capabilities of pyFormex and the solving power of ABAQUS, we can easily test the effect of many parameters in a minimal amount of time, which is useful because a lot of parameters are particularly difficult to obtain for seahorse's anatomy and are lacking in literature.

4. SIMULATION RESULTS

In all following simulations, the muscle contraction is simulated by a change in connector length with an amplitude $A(t)$ that follows a smooth step (Equation 1), so that the contraction acceleration is continuous, initial contraction speed is zero, and final contraction speed is zero:

$$A(t) = -2t^3 + 3t^2, \quad t = 0, \ldots, 1. \tag{1}$$

Kinetic energy (from inertial forces) is kept negligible compared with potential energy (stored in the joints and later on in passive muscles) at each time increment. The vertebra of the first segment of the tail is kept fixed, and the most proximal points of the dermal plates of the first segment are

DOI: 10.1002/cnm

connected by an additional stiff joint to account for the connection with the rest of the seahorse skeleton. The tail tip is modelled by a single rigid body, as demonstrated in Figure 8(B).

4.1. Median ventral muscle contraction

Figure 10 gives an example of ventral tail bending powered by MVM contraction. Usually, the seahorse tail will bend non-uniformly (with distal muscles contracting more than proximal muscles). This natural tail bending was simulated here, by varying the total muscle contraction linearly through the tail MVM, from 0% for the most proximal MVM to 50% for the most distal MVM. The final shape of the centreline of the tail approximates a logarithmic spiral.

Simulations with contraction of all MVM to an assumed maximum contraction were also performed (Figure 11). These results are then compared with measurements on a tail that was manually manipulated to maximum bending (so this is passive tail bending, in contrast to the active tail bending of the simulations) (Figure 11). These measurement were taken from a previous study [16]. In the simulation, a constant MVM contraction of 30% was taken. Higher contractions will lead to collision of the tail segments: the most proximal segments will collide with the segments that are further down the tail. The MVM are, however, assumed to be able to contract more than 30%, presumably up to 50%. This indicates that the maximal ventral tail contraction is limited by geometrical constraints, rather than muscle contraction constraints.

The geometric limitation for ventral tail bending is also supported by the notion that the gliding joints between sequential dermal plates will lock at a certain intrusion because the proximal groove of the more distal plate ends rather abruptly. The distance of this intrusion can be measured as the distance between the most distal point of the distal spine and the end of the groove of the subsequent plate. For the ventral dermal plates (that become compressed upon ventral bending), this distance is measured to be on average 18.7% of the segment length (with a standard deviation of 3.1%). The model suggests that this compression of the lateral–ventral gliding joints would occur at 27.1%

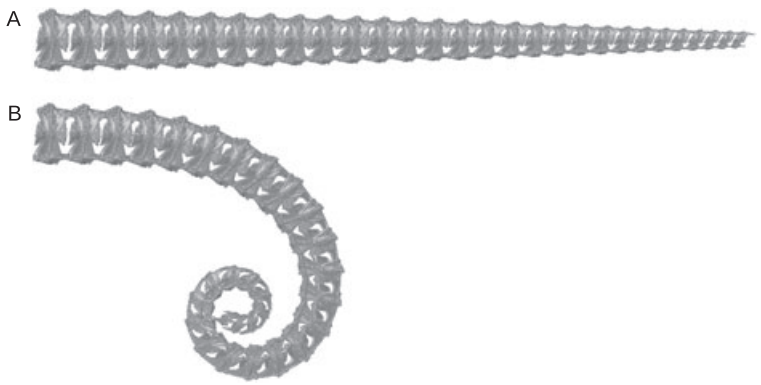

Figure 10. Simulated tail bending before (A) and after (B) contracting the median ventral muscles.

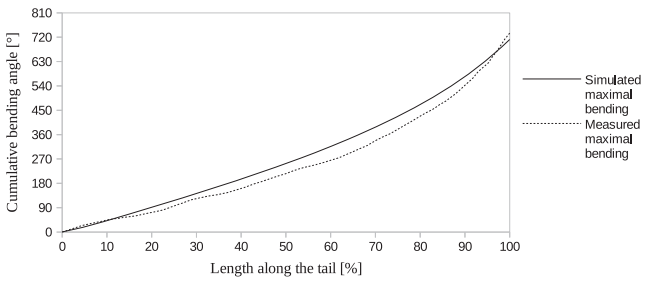

Figure 11. Comparison of maximal ventral tail bending upon contraction of the MVM in measurement and simulation.

DOI: 10.1002/cnm

contraction of the MVM. This is in good agreement with the only values for maximal MVM contractions found in literature: 26.7%, with a standard variation of 4.5% [11]. These maximal contraction values of the MVM were measured in the more distal segments of live seahorses, that tightly held on to a support with a small diameter. That same study mentioned that high contraction of the anterior MVM is not observed in living seahorses [11].

During tail bending, the lateral gliding joints become slightly compressed, whereas the ventral gliding joints within one segment get stretched, as indicated in Figure 12. The dorsal joints within one segment do not change much, as their movement is limited by their mutual joints with the central vertebra.

4.2. Hypaxial myomere muscle contraction

Both unilateral and bilateral HMM contraction were modelled within the versatile dynamic model. As suspected, bilateral contraction will cause a purely ventral bending, whereas unilateral contraction will cause a combined ventral–lateral tail bending. As the hypaxial myosepta span several vertebrae, it is unlikely that HMM contraction can cause significantly different bending in adjacent segments. We therefore use an equal amount of contraction for all HMM. When unilateral HMM contraction is applied to the model, the dynamic analyses show a lateral displacement that is around four times larger than the ventral displacement (Figure 13). This shows the maximal lateral tail displacement, compared with the ventral displacement, that a seahorse could obtain using only the ventral muscles. By compensating with the epaxial myomere muscles, the seahorse can obtain a higher lateral bending. These muscles are not yet included in the current model.

4.3. Missing dermal plate

Personal observations showed that, in some seahorses, a few ventral dermal plates are missing, apparently without compromising the proper functioning of the seahorse tail. Whether the malformation of the skeleton is a result of an injury, genetics or environment is currently unknown. To

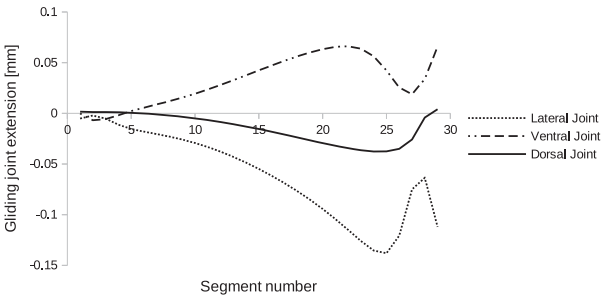

Figure 12. Extension of the intrasegmental gliding joints throughout the tail. Positive values are extension; negative values are compression.

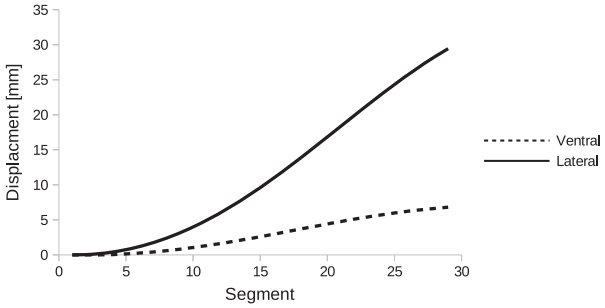

Figure 13. Ventral and lateral displacement of the tail segments upon uniform unilateral contraction of the HMM.

DOI: 10.1002/cnm

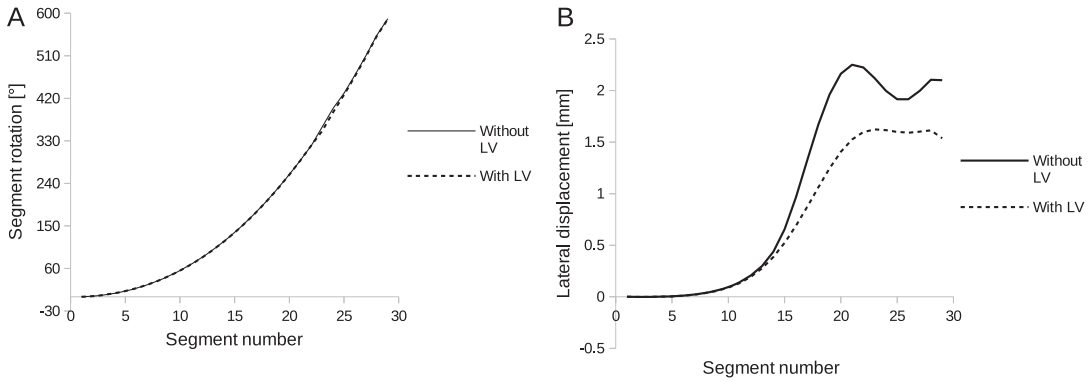

Figure 14. Bending angle (A) and lateral displacement (B) of the tail segments with and without the left ventral dermal plate (LV) of the 15th segment removed. Displacement of the tail is to the side of the missing plate.

check the effect of one missing ventral dermal plate on the dynamics, a model was created where one left ventral dermal plate was removed. As hypothesised, the effect on the ventral bending of the tail was small (Figure 14(A)), although some additional torsion of the tail was noticed distally from the missing skeletal element, as well as an additional lateral displacement of the segments distal from the absent element (Figure 14(B)). This is not surprising, given the local asymmetry of the model, caused by the missing dermal plate.

5. DISCUSSION

Literature on kinematic and dynamic simulations on fish mainly focuses on swimming kinematics for robotic applications [25–29]. In contrast to most fish, the seahorse does not use its tail for swimming, but rather for grasping and holding. Therefore the kinematics of the tail movement is very distinct, making a comparison with other numerical methods in fish simulations difficult. There has been a study on the grasping of octopus arms, but the kinematics of these arms are determined purely by muscles [30, 31]. Because there is no skeleton involved in the kinematics of the octopus arm, comparison of methodology is again difficult.

To fully understand the mechanics involved in the combination of radial stiffness and bending flexibility of the seahorse tail, all skeletal elements of the seahorse tail needed to be included in the model. Therefore, a simplified dynamic model of the seahorse tail was constructed. Because no data on muscle activation or reaction forces were available, muscle contraction was modelled using shortening of connectors between the attachment points of the muscles. In this way, the model allows us to simulate ventral and combined ventral–lateral tail bending. Currently, all potential energy is stored in the joints, rather than in the passive muscles on the dorsal side of the tail. These passive epaxial muscles will be added to the model shortly. The elasticity of the joints is currently loosely approximated, although all elasticity values are parametric, so future stiffness measurements can easily be incorporated into the model. The rest of the model generation is also kept parametric so that several features, such as the skewness and size of the segments, can be altered and their effect on the dynamics quantified. The model needs some optimization and fine-tuning before evolutionary conclusions can be drawn from the parametric results. Nevertheless, results seem promising and robust: for most parameter changes the displacements and velocities are only mildly affected. Clearly the lack of input data on muscle forces and reaction forces does not yet allow us to draw quantitative conclusions from the simulation results.

The joint compressions in Figure 12 show that within one segment the lateral joints and the dorsal joints get compressed upon ventral bending of the tail, whereas the ventral joints elongate. As the transverse intersection of the stretched tail is almost shaped like a square, the net effect of the joint movements within one segment is a slight decrease in cross-sectional area upon tail bending. The

DOI: 10.1002/cnm

internal volume of the seahorse tail should, however, remain almost constant during bending, as the compressibility of soft tissues is normally quite low. Moreover, when we consider the tail to be a bending beam, the rotational centre around which the vertebrae rotate is surprisingly not located on the neutral axis (which is on the frontal plane), but a bit more dorsal. This means that upon ventral tail bending, the cross-sectional area should even increase slightly to avoid a change in volume of the soft tissues in between. The total change in volume in our simulation is typically low, but still, the seahorse tail model should take the influence of the soft tissues between the bony elements into account to obtain more realistic results.

During tail bending, the gliding joints in the corners of the segments seem to play a vital role in supporting the flexibility of the tail. At ventral tail bending, the ventral longitudinal joints compress, whereas the dorsal longitudinal joints expand. In this way, the armour plating that covers the tail can bend extensively without losing its integrity, or without large changes in internal volume. As for the radial stiffness, the geometry of the central vertebra appears to play a vital role in coping with the external forces. Through ball-and-socket joints, the central vertebra supports the large dorsal dermal plates, and thus copes with the radial forces, which would otherwise just compress the lateral and dorsal gliding joints. The ventral dermal plates seem to play a less vital role in the tail dynamics and radial stiffness resistance. This was supported by removing a ventral plate in the model, after which displacements of skeletal elements and general curling of the tail was only minorly affected. More study on improved models, including contact and deformable bodies, is being conducted to fully support these conclusions.

Despite the current limitations, results of the model seem promising when compared with values in literature, as can be seen for the predicted muscle contraction at maximal compression of the ventral longitudinal joints, as well as the predicted maximal ventral bending upon MVM contraction (Figure 11). As a first step towards fully understanding the biomechanics of the seahorse tail, this model takes us a long way.

6. CONCLUSIONS

In this paper, we presented a strategy to construct a versatile dynamic model of the musculoskeletal system of the seahorse tail. The large number of skeletal elements (and thus joints) in the seahorse tail, combined with the inability to obtain muscle activation sequences, led us to develop a less common modelling strategy. Using multi-body simulations that are generated using pyFormex scripts, we obtained a better insight in seahorse tail dynamics. MVMs and HMMs can be activated and their effect on tail bending quantified. The model suggests realistic values for maximal contraction of the MVMs. It also shows that the absence of a single ventral dermal plate has little effect on the dynamics of the tail, although the HMMs exert force on them by the thick ventral tendons.

How these findings can contribute in the design of biomedical (and possibly other) devices will be studied later on. The complexity of the seahorse tail (in geometry, amount of joints, influence of soft tissues, large amount of muscles, ...) makes it challenging to apply the same principles in engineering.

ACKNOWLEDGEMENTS

We would like to gratefully acknowledge the Centre for X-ray Tomography (UGCT) of Ghent University for providing the μ-CT scans of the *Hippocampus reidi* specimens, as well as the European Synchrotron Radiation Facility in Grenoble (Renaud Boistel, Université de Poitiers) for providing the synchrotron scans. This research was funded by the Research Foundation Flanders (FWO Vlaanderen), grant number G.0137.09N.

REFERENCES

1. Quinn S, Gaughran W. Bionics—an inspiration for intelligent manufacturing and engineering. *Robotics and Computer-Integrated Manufacturing* 2010; **26**(6):616–621.
2. Peters K, Johansson A, Dussutour A, Helbing D. Analytical and numerical investigation of ant behavior under crowded conditions. *Advances in Complex Systems* 2006; **9**:337–352.

DOI: 10.1002/cnm

3. Raibeck L, Reap J, Bras B. Investigating environmental burdens and benefits of biologically inspired self-cleaning surfaces. *CIRP Journal of Manufacturing Science and Technology* 2009; **1**:230–236.
4. Coelho LdS, Mariani VC. Use of chaotic sequences in a biologically inspired algorithm for engineering design optimization. *Expert Systems with Applications* 2008; **34**(3):1905–1913.
5. Teske PR, Cherry MI, Matthee CA. The evolutionary history of seahorses (Syngnathidae: Hippocampus): molecular data suggest a West Pacific origin and two invasions of the Atlantic Ocean. *Molecular Phylogenetics and Evolution* 2004; **30**:273–286.
6. Teske PR, Beheregaray LB. Evolution of seahorses' upright posture was linked to Oligocene expansion of seagrass habitats. *Biology Letters* 2009; **5**:521–523.
7. Van Wassenbergh S, Roos G, Ferry L. An adaptive explanation for the horse-like shape of seahorses. *Nature Communications* 2011; **2**(164):1–5.
8. Consi TR, Seifert PA, Triantafyllou MS, Edelman ER. The dorsal fin engine of the seahorse (Hippocampus sp.) *Journal of Morphology* 2001; **248**:80–97.
9. Bruner E, Bartolino V. Morphological Variation in the seahorse vertebral system. *International Journal of Morphology* 2008; **26**(2):247–262.
10. Breder CM, Edgerton HE. An analysis of the locomotion of the seahorse, Hippocampus, by means of high speed cinematography. *Annals of the New York Academy of Sciences* 1942; **XLIII**(4):145–172.
11. Hale ME. Functional morphology of ventral tail bending and prehensile abilities of the seahorse, Hippocampus kuda. *Journal of Morphology* 1996; **227**:51–65.
12. Perante NC, Pajaro MG, Meeuwig JJ, Vincent ACJ. Biology of a seahorse species, Hippocampus comes in the central Philippines. *Journal of Fish Biology* 2002; **60**:821–837.
13. Peters HM. Beiträge zur Ökologischen Physiologie des Seepferdes (Hippocampus Brevirostris). *Zeitschrift für vergleichende Physiologie* 1951; **33**:207–265.
14. Weber H. Beiträge zur Bewegungsphysiologie der Hippocampus-Arten. *Zeitschrift für vergleichende Physiologie* 1927; **5**(1):1–36.
15. Anthony R, Chevroton L. Considérations sur les attitudes et la locomotion de l'hippocampe, étude chronophotographique. *Archives de zoologie, notes et revues* 1913; **51**:11–22.
16. Neutens C. Evolutionary morphology of the prehensile tail in seahorses (Sygnatidae, Hippocampus): a microscopical-anatomical 3D study. *Master thesis*, Ghent University, 2011.
17. Van Cauter S, Adriaens D, Kannan S, Srigiriraju S, Praet T, Masschaele B, De Beule M, Verhegghe B. Virtual design from nature: kinematic modeling of the seahorse tail. *2010 SIMULIA Customer Conference Proceedings*, Providence, RI, USA, 2010; 770–783.
18. Gemballa S, Vogel F. Spatial arrangement of white muscle fibres and myoseptal tendons in fishes. *Comparative Biochemistry and Physiology Part A* 2002; **133**:1013 –1037.
19. Van Leeuwen JL. A mechanical analysis of myomere shape in fish. *The Journal of Experimental Biology* 1999; **202**:3405 –3414.
20. Vogel F, Gemballa S. Locomotory design of 'cyclostome' fishes: spatial arrangement and architecture of myosepta and lamellae. *Acta Zoologica* 2000; **81**:267 –283.
21. Neutens C, Adriaens D, Christiaens J, De Kegel B, Dierick M, Boistel R, Van Hoorebeke L. Grasping convergent evolution in sygnathids: a unique tale in tails. *Proceedings of the Royal Society B*, Submitted.
22. Vollmer J, Mencl R, Muller H. Improved Laplacian smoothing of noisy surface meshes. *Computer Graphics Forum* 1999; **18**(3):131–138.
23. Biltz RM, Pellegrino ED. The chemical anatomy of bone: I. A comparitive study of bone composition in sixteen vertebrates. *The journal of bone and joint surgery* 1969; **51**(3):456–466.
24. Horton JM, Summers AP. The material properties of acellular bone in a teleost fish. *The Journal of Experimental Biology* 2009; **212**:1413 –1420.
25. Zhou C, Tan M, Cao Z, Wang S, Creighton D, Gu N, Nahavandi S. Kinematic modeling of a bio-inspired robotic fish. *2008 IEEE International Conference on Robotics and Automation*, Pasadena, CA, USA, 2008; 695–699.
26. Liu J, Hu H. Biological inspiration: from carangiform fish to multi-joint robotic fish. *Journal of Bionic Engineering* 2010; **7**:35–48.
27. Yu J, Tan M, Wang S, Erkui C. Development of a biomimetic robotic fish and its control algorithm. *IEEE Transactions on Systems, Man, and Cybernetics—Part B: Cybernetics* 2004; **34**(4):1798–1810.
28. Chen Z, Shatara S, Tan X. Modeling of biomimetic robotic fish propelled by an ionic polymermetal composite caudal fin. *IEEE/ASME Transactions on Mechatronics* 2010; **15**(3):448–459.
29. Siahmansouri M, Ghanbari A, Fakhrabadi MMS. Design, implementation and control of a fish robot with undulating fins. *International Journal of Advanced Robotic Systems* 2011; **8**(5):61–69.
30. Laschi C, Mazzolai B, Mattoli V, Cianchetti M, Dario P. Design of a biomimetic robotic octopus arm. *Bioinspiration & Biomimetics* 2009; **4**:1–8.
31. Calisti M, Giorelli M, Levy G, Mazzolai B, Hochner B, Laschi C, Dario P. An octopus-bioinspired solution to movement and manipulation for soft robots. *Bioinspiration & Biomimetics* 2011; **6**:1–10.

DOI: 10.1002/cnm